http://dx.doi.org/10.5935/0103-5053.20130137
J. Braz. Chem. Soc., Vol. 24, No. 6, 1064-1071, 2013.
Printed in Brazil - ©2013 Sociedade Brasileira de Química
0103 - 5053 $6.00+0.00

Article

Thermodynamic Simulation of Phosphate Precipitation based on Ion-Selective Microelectrode Measurements

Gustavo M. Platt,[a] Ivan N. Bastos,[a] Mônica C. de Andrade,[a] Marina Taryba,[b] Sviatlana V. Lamaka[b], Alda Simões[b] and Glória D. Soares*[,c]

[a]*Instituto Politécnico, Universidade do Estado do Rio de Janeiro, 28625-570 Nova Friburgo-RJ, Brazil*

[b]*Instituto de Ciência e Engenharia de Materiais e Superfícies, Instituto Superior Técnico, Av. Rovisco Pais, 1049-001 Lisboa, Portugal*

[c]*Departamento de Engenharia Metalúrgica e de Materiais, Universidade Federal do Rio de Janeiro, 21941-972 Rio de Janeiro-RJ, Brazil*

Soluções simuladoras do fluido corpóreo (SBFs) são usadas em avaliação de biocompatibilidade de biomateriais e também como processo de recobrimento alternativo à aspersão por plasma. Processos biomiméticos ocorrem heterogeneamente sobre superfícies metálicas; portanto, o uso da técnica de microeletrodo é muito recomendável para detectar mudanças na superfície. Neste trabalho, o pH local foi monitorado durante as primeiras 44 h de deposição de fosfato de cálcio em amostras de titânio com uma solução SBF simplificada. Dados tridimensionais (pH local, coordenadas *x*-*y*) foram empregados para simular as concentrações de equilíbrio para todas as espécies químicas. Baseadas nestas quantidades, foram calculadas as supersaturações relativas e variações de energia de Gibbs para hidroxiapatita e fosfato octacálcico. A abordagem experimental e teórica conjunta sugere que nem a alcalinidade local nem a concentração de cálcio livre fornecem um cenário adequado sobre a condição de precipitação, mas o uso simultâneo produz resultados interessantes não obtidos com somente uma delas.

Simulated body fluids (SBFs) are largely used as biocompatibility screening and also as an alternative process to the plasma spray coating. Biomimetic processes occur heterogeneously on metallic surface; therefore, the use of a microelectrode technique is highly advisable to detect surface changes. In this work, the local pH was monitored during the first 44 h of deposition of calcium phosphates on titanium samples with a simplified SBF solution. Three-dimensional data (local pH, *x*-*y* coordinates) were used to simulate equilibrium concentrations of all species. Based on these quantities, relative supersaturations and Gibbs energy variations of hydroxyapatite and octacalcium phosphate were evaluated. The conjoint experimental and theoretical approach suggested that neither local alkalinity nor free calcium concentration alone produces an adequate scenario of precipitation conditions, but the use of both procedures results in interesting findings not achieved using only a single approach.

Keywords: ion-selective microelectrode, hydroxyapatite, local pH, biomimetic precipitation

Introduction

Multicomponent reactions take place in diverse physical systems of great interest, such as natural water, biological fluids and, consequently, in biomimetic processes.[1] In these cases, the simultaneous equilibrium of dozens of species can generally only be simulated by numerical procedures. SBFs are a good example of these.[2-4]

Biomimetic processes are heavily used in bioactivity testing of metallic surfaces for biomedical applications.[5] Despite their extensive use, few works have focused on theoretical aspects of thermodynamic or evolution behavior that could give additional information not available in clinical evaluations.[2,6]

In the present work, titanium surfaces were coated with a designed simplified SBF solution whose chemical composition is based on the ionic species necessary to form calcium phosphates, e.g., calcium and phosphate ions in

*e-mail: gloria.soares@gmail.com

dilute aqueous solution.[4] Besides the advantage of easy preparation, a less complex composition simplifies the understanding of simultaneous chemical reactions.

Biomimetic precipitation on metallic implants is a heterogeneous reaction, and the precise evaluation of physicochemical parameters as close as possible to the surface is of prime importance to understand the system. SIET (scanning ion-selective electrode technique) is a local technique that allows measurements of the chemical composition very close to a surface. It was previously used to study the flux of ions in cell membranes, and further applied to Materials Science.[7-10] However, for biomimetic precipitation, this technique, as far as we can see, has not been employed. One advantage of the local pH measurement in the *in vitro* situation is the possibility of following the evolution behavior and applying thermodynamic modeling, because the system is simpler than an *in vivo* case. Therefore, our group performed an experimental test under biomimetic conditions, without buffers, and the earliest time points (up to 44 h) of local pH evolution were monitored. From these data, chemical equilibrium calculations were conducted in order to obtain the concentrations of other species (such as free calcium and phosphates) as well as the Gibbs energy variations and supersaturations for calcium phosphates with biomedical interest. The main objective of this work is to propose an integrated tool (SIET + computational simulations) in order to gain access to some important thermodynamic quantities useful for prediction of calcium phosphate formation with biomedical interest.

Experimental

Titanium samples (8 mm × 8 mm) were cut from a biomedical grade titanium sheet (American Society for Testing and Materials Standard ASTM F67-89). The sample was embedded in an inert epoxy holder and polished with emery paper up to 1200 mesh. After the polishing, the samples were exposed to air, and the formation of titanium oxide took place. The cleaning process obeyed the following sequence: cleaning with MilliPore purified water under ultrasound waves for 3 min; washing with alcohol plus ultrasound for 3 min, and finally immersion in water plus ultrasound for 3 min. To decrease the area of the metallic surface exposed to solution and hence increase the resolution of the pH mapping, the metallic surface was covered with bee wax except for an area of 3 mm × 3 mm.

The simplified solution was designed using a computational simulator named SimSE (Electrolyte Solution Simulator).[2] This solution was prepared with the following reagents (pure for analysis grade obtained from Merck): $NaHCO_3$, K_2HPO_4, $CaCl_2.2H_2O$ and MilliPore filtered water ($\rho > 18$ MΩ cm), in order to obtain the following total ionic concentrations (in mmol L^{-1}): 2.5 Ca^{2+}, 5.0 Cl^-, 4.2 Na^+, 4.2 HCO_3^-, 2.0 K^+ and 1.0 HPO_4^{2-}. The solution was prepared just before the pH-SIET tests. The temperature of the solution was maintained at 298.15 K during preparation. The solution volume was 6.4 cm^3, and the exposed area was 0.09 cm^2. Thus, the ratio solution volume/exposed surface is approximately 71 cm^3 cm^{-2}. The experiments were performed in duplicate.

Commercial equipment manufactured by Applicable Electronics and controlled by Aset software was used to perform SIET measurements. The SIET pre-amplifier was mounted on 3D step motors that moved with a lateral resolution of 0.8 μm and were used to position a pH microelectrode over the active surface. Localized pH measurements were performed using a glass-capillary ISME (ion-selective microelectrode). The pH selective microelectrodes were prepared from single-barrelled, standard-wall (330 μm) borosilicate glass capillaries with an outer diameter of 1.5 mm. A P-97 Flaming/Brown Micropipette Puller (Sutter Instruments) was used to shape the cone tip. The diameter at the apex of the tip was 2.0 ± 0.5 μm. Before use, the inner surface of each capillary was silanized by injecting 200 μL of *N*,*N*-dimethyltrimethylsilylamine in a glass preparation chamber at 200 °C. The silanized capillaries were filled with a selective ionophore-based oil-like membrane and back-filled with an inner reference solution. The column length of the membrane was about 60-70 μm. The pH-SME (pH selective microelectrode) membrane consisted of 6 wt.% ETH 1907 (4-nonadecylpyridine), 12 mol% (relative to the ionophore) potassium tetrakis(4-chlorophenyl) borate, and a membrane solvent, 2-nitrophenyloctyl ether. All reagents for the pH-SME membrane were Selectophore grade products from Fluka. pH-SME was calibrated using commercially available pH buffers. The linear range of the pH response was 2-10, and the nernstian slope was −51.3 mV pH^{-1}. All experiments were performed in a Faraday cage at room temperature. A "move-wait-measure pH" scheme was employed for mapping above the surface. The time for acquisition for each pH data-point was 1.5 s. For the presented SIET-pH measurements, pH-SME was fixed at a height of 50 ± 10 μm above the surface. All measurements were carried out in an SBF solution. Frames of *circa* 2 mm × 2 mm measurements were consecutively performed at each hour, up to 44 h of exposure. Measurements were performed in a 31 × 31 grid, generating 961 points. The measuring steps were 73 μm (*x* direction) and 60 μm (*y* direction). A region of this frame was reserved to measure the change close to the wax to allow comparison with the titanium surface effect. Besides continuous image

monitoring, low magnification optical images of the surface were taken at a rate of one picture *per* hour. These maps were used to simulate the presence of other ions in equilibrium, as presented in the following section.

Theoretical analysis

Using the local pH measurements, several equilibrium calculations were undertaken in order to access thermodynamic quantities such as ionic concentrations (and activities), relative supersaturations and Gibbs energy variations (between a supersaturated solution and the saturation condition). For this task, the following equilibrium reactions in a liquid phase were considered:
(*i*) Water equilibrium

$$H^+ + OH^- \rightleftharpoons H_2O \quad (1)$$

(*ii*) Protonation/deprotonation of phosphates

$$H^+ + PO_4^{3-} \rightleftharpoons HPO_4^{2-} \quad (2)$$
$$H^+ + HPO_4^{2-} \rightleftharpoons H_2PO_4^- \quad (3)$$
$$H^+ + H_2PO_4^- \rightleftharpoons H_3PO_4 \quad (4)$$

(*iii*) Calcium ion equilibria

$$Ca^{2+} + HPO_4^{2-} \rightleftharpoons CaHPO_4 \text{ (aqueous)} \quad (5)$$
$$Ca^{2+} + H_2PO_4^- \rightleftharpoons CaH_2PO_4^+ \quad (6)$$
$$Ca^{2+} + OH^- \rightleftharpoons CaOH^+ \quad (7)$$
$$Ca^{2+} + PO_4^{3-} \rightleftharpoons CaPO_4^- \quad (8)$$
$$Ca^{2+} + CO_3^{2-} \rightleftharpoons CaCO_3 \text{ (aqueous)} \quad (9)$$
$$Ca^{2+} + HCO_3^- \rightleftharpoons CaHCO_3^+ \quad (10)$$

(*iv*) Carbonate/bicarbonate equilibrium

$$HCO_3^- \rightleftharpoons H^+ + CO_3^{2+} \quad (11)$$

Besides these chemical equilibrium reactions, it was taken into account the material balances for phosphorus, calcium and carbon. Activity coefficients for charged species were calculated for long-range interactions, using the extended Debye-Hückel model and the Bates-Guggenheim convention for chloride ion.[11] Detailed explanations of chemical equilibrium modeling and numerical aspects of SBF simulations are presented in Bastos *et al.*[2] Equilibrium constants for reactions 2-11 are found in the references.[3,12-14]

For pH specification, the nonlinear algebraic system formed by chemical equilibrium equations 1-11 and material balances must be solved in order to access ionic concentrations and activities at equilibrium conditions.

A designed computational simulator (SimSE) was used with some modifications to enable compatibility with the three-dimensional SIET data (local pH, *x-y* coordinates) provided by pH-SME (essentially, a double-loop structure in order to scan all points in the surface).[2] The numerical procedure is based on a damped Newton method with Jacobian matrix calculated by forward finite-differences. This new version of SimSE is able to produce ionic concentration maps (and additional thermodynamic quantities such as Gibbs energies for precipitation, expressing the deviations from equilibrium).

Within this framework, chemical equilibrium assumptions for a liquid phase are considered at all instants to emulate the actual phenomenon (not considering kinetic aspects). This approach is useful in order to estimate the driving forces for precipitation processes.[15] Another important assumption in this model is that the total quantities of calcium, phosphate (and its protonated/complex forms) and bicarbonate (and its forms, including carbonate) are considered constant during the precipitation process (the material balances in the liquid phase are maintained). In other words, this means that the quantity of solid phase is negligible when compared with the ionic quantities available in solution. The hypothesis of a closed *in vitro* system has great advantages over *in vivo* systems, which are open. This consideration is very important in mass balance equations. With calculated values for ionic concentrations/activities, Gibbs energies for precipitation were calculated for octacalcium phosphate (OCP) and hydroxyapatite (HA). For instance, the following precipitation reaction for hydroxyapatite was considered:

$$5Ca^{2+} + 3PO_4^{3-} + OH^- \overset{K_{SP,HA}}{\rightleftharpoons} Ca_5(PO_4)_3(OH) \quad (12)$$

Thus, the Gibbs energy variation between the supersaturated and saturated solution (ΔG_{HA}, for hydroxyapatite) is given by

$$\Delta G_{HA}(\text{J mol}^{-1}) = -\frac{RT}{9}\ln\left(\frac{IAP}{K_{SP,HA}}\right), \quad (13)$$

where IAP refers to the ionic activity product (calculated using SimSE), T is the absolute temperature (K), R is the universal gas constant (J mol^{-1} K^{-1}) and $K_{SP,HA}$ is the solubility product constant for hydroxyapatite at 298.15 K. Analogous numerical procedures can be extended for other calcium phosphates, but octacalcium phosphate and hydroxyapatite were chosen due to their importance as bioceramics. Besides, only hydroxyapatite, octacalcium phosphate and calcium-deficient hydroxyapatite are possible in the considered pH range.[16] Since consistent

values for substitution of phosphate by hydrogen phosphate ions in calcium-deficient hydroxyapatite were not obtained, calculations for this phosphate were not performed. Thus, the solubility constant product for this phosphate is inaccurate.[16] Solubility product constants for hydroxyapatite and octacalcium phosphate were found in Glinkina *et al.*[3] and Tung *et al.*,[17] respectively.

The relative supersaturations (referred hereafter as supersaturations) are also presented, being defined as:

$$\sigma = \left(\frac{IAP}{K_{SP}} \right)^{1/n} - 1, \qquad (14)$$

where n is the sum of stoichiometric coefficients for HA or OCP precipitations.

In all figures depicted in the following section, the x-y coordinates are expressed in μm; the free Gibbs energy in J mol^{-1}; and the chemical concentrations in mol L^{-1}, except for pH that is traditionally expressed as –log [H^+]. The brightness of the maps varies with each specific scale.

Results and Discussion

Figure 1 presents an initial map of local pH measured just after immersion of the titanium in SBF solution. The first measured point is located at top-left position and the last one at bottom-right position. The lateral region corresponds to the bee wax. This configuration of measurement is interesting for revealing the effect of a metallic surface when compared with an inert surface. It is worth noting that completing one map demands *circa* 40 min, thus the instant of measurement increases to the right or below directions. The drift of the potential of the pH-selective microelectrode did not exceed 0.5 mV h^{-1} during the measurements. Reproducibility of the potential was 0.3 mV.

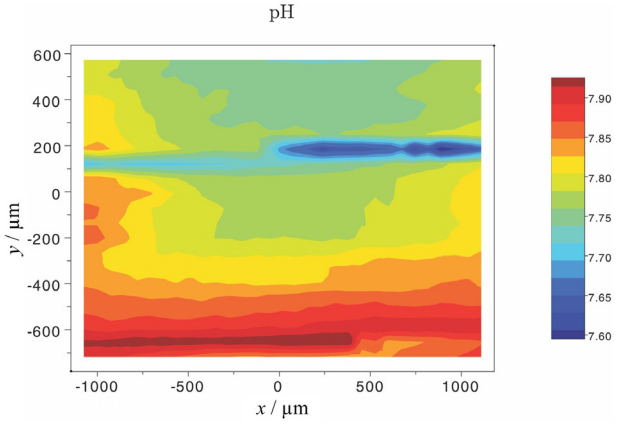

Figure 1. Map of local pH measured just after the immersion. Values along the x- and y-axes show the relative position of pH-SME in μm. The size of the x-y scan was 2200 × 1320 μm, respectively.

Figure 2 shows the maximum, minimum and average (considering all measured points in the surface) local pH for all measured instants, corresponding to titanium and wax, up to 44 h. The average pH begins close to 8 and reaches its maximum in the first moments of the process. Subsequently, there is a slow decay in values up to the end of the experimental exposure. The extreme values (maximum and minimum) follow a similar scattering.

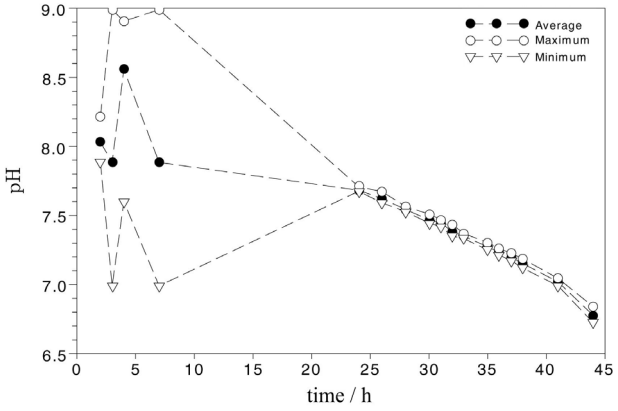

Figure 2. Evolution of local pH measured on titanium and wax for 44 h.

The following results (Figure 3) are related to thermodynamic calculations. All numerical evaluations correspond to the liquid phase. For example, Gibbs energies are related to the difference between supersaturated solutions (an unstable equilibrium condition, with calculated activities/concentrations) and the saturation condition (evaluated by solubility constant products for a given solid phase). Figure 3 presents the calculated concentrations for Ca^{2+}, $CaPO_4^-$, CO_3^{2-} and HCO_3^-. All variables (concentrations, activities, activity coefficients, etc.) are available, but for the sake of conciseness only the most relevant are shown.

Calcium ions are extremely important in the apatites for biomedical applications.[16] $CaPO_4^-$ is a highly stable calcium phosphate complex and its concentration affects free calcium availability.[2,13] Carbonate/bicarbonate equilibrium is strongly dependent on pH and must be monitored during deposition. Supersaturations and Gibbs energies for precipitation of octacalcium phosphate and hydroxyapatite are also shown.

A horizontal "line" between the titanium and wax can be observed in all maps after 4 h (Figure 3), with a reduced pH. For instance, if the coordinates (x, y) = (–887, –424) are considered, the local pH is close to 8.9. Maintaining the x-coordinate at –887 μm, but considering y = –636 μm (titanium-wax interface), the pH is near 7.6. This pH behavior is also reflected on other maps. For all x-coordinate values at y = –636 μm, calcium concentration is increased

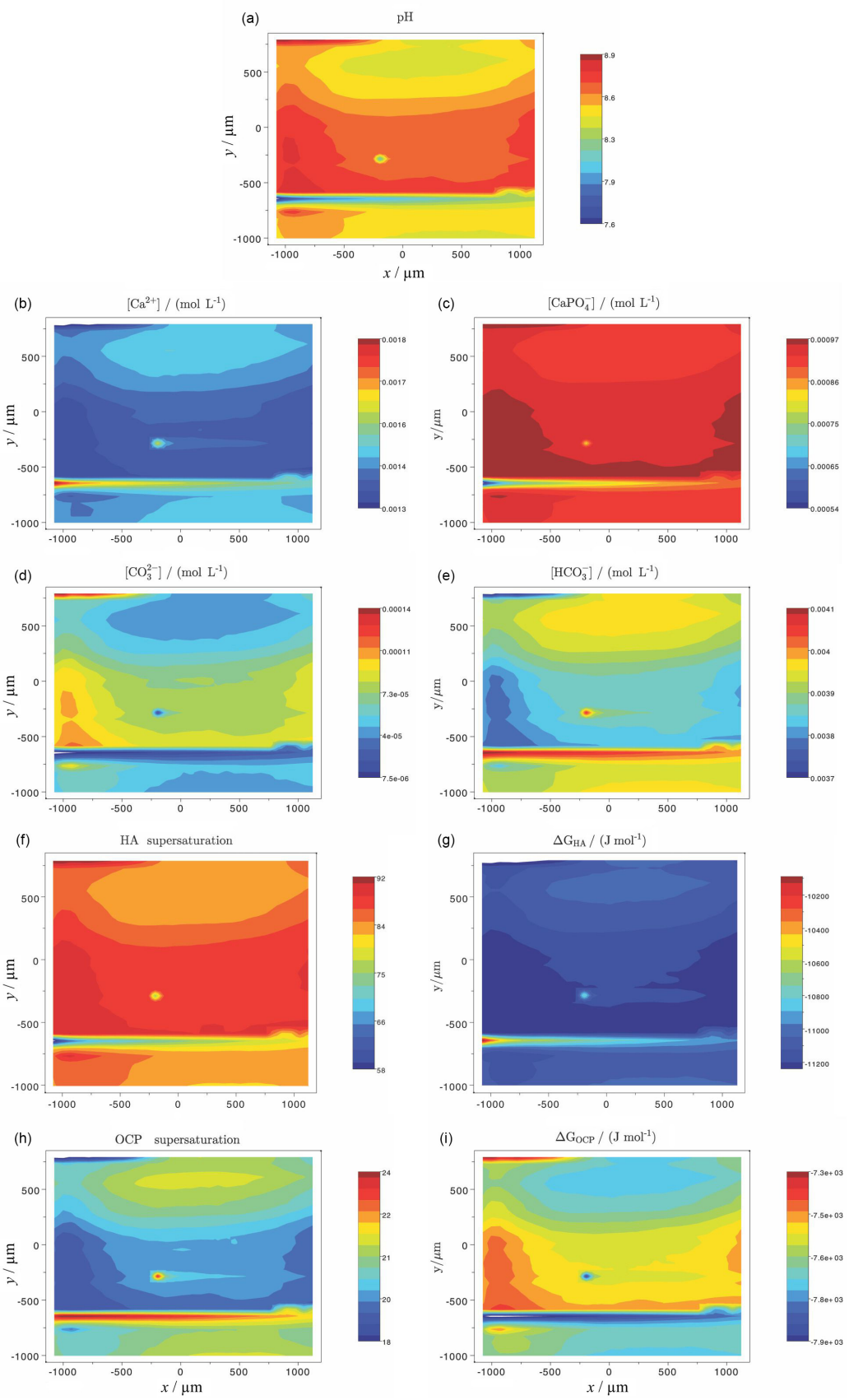

Figure 3. Experimental (local pH) and equilibrium theoretical maps after 4 h. Experimental: (a) local pH. Theoretical evaluations: (b) $[Ca^{2+}]$, (c) $[CaPO_4^-]$, (d) $[CO_3^{2-}]$, (e) $[HCO_3^-]$, (f) HA supersaturation, (g) HA Gibbs energy, (h) OCP supersaturation and (i) OCP Gibbs energy.

to 0.0018 mol L^{-1}. This difference could be ascribed to a lateral flux of calcium ions since the surface diffusivity is high; although feasible, this flux was not estimated as it has already been done in the literature.[7]

For a multicomponent system governed by a nonlinear set of equations, the measurement of a single parameter is normally insufficient to give a proper status of the system. Indeed, the present findings agree with this general consideration. For a given point in the surface, a high free calcium concentration corresponds to a low pH value (Figures 3a and 3b). Anyway, for hydroxyapatite precipitation, the increase of free calcium concentration is desirable (equation 12). However, even for a high free calcium concentration, at a low pH point, a high HA supersaturation is not observed. This combined effect is shown by supersaturations and Gibbs energies: for octacalcium phosphate, this "line" represents the more stable condition for precipitation; for hydroxyapatite, the corresponding region shows fewer tendencies to form a solid phase (lower availability of OH^- as a consequence of low pH). These calculated results are fully compatible with experimental findings; lower pH promotes octacalcium phosphate phase deposition, and an increase in pH provokes the formation of hydroxyapatite. Moreover, the supersaturation and the corresponding free Gibbs energy variation, obtained from experimental (pH-SME) as well as theoretical calculations (thermodynamics), give a more understandable picture of the local driving force for apatite precipitation. Thus, an increase in free calcium availability is desirable from the point of view of octacalcium phosphate and hydroxyapatite formation, but the dependency of other parameters on precipitation indicates that quantitative estimation of the driving force is only feasible with experimental and numerical approaches.

Some scattering in local pH is a result of experimental effects (see, for instance, the "dark point" in the pH map close to x = –200 µm, y = –260 µm in Figure 3a). Despite extreme caution during the experiments, several factors could produce this small perturbation: metallic heterogeneity, electronic noise, vibration, etc. However, this experimental artifact did not jeopardize the maps obtained with a very large number of points.

Figure 4 shows the local pH map after 44 h. In this situation, there is a tendency toward pH homogenization on the titanium surface. In all subsequent maps, it is possible to consider that there are no significant variations for all thermodynamic quantities as functions of x, y position. For sake of conciseness, these maps were not presented, but the representative quantities for an average pH, approximately equal to 6.8, are exhibited. For this pH, $[Ca^{2+}]$ = 0.0022 mol L^{-1}, $[CaPO_4^-]$ = 0.0001 mol L^{-1}, $[CO_3^{2-}]$ = 0.0000012 mol L^{-1}, $[HCO_3^-]$ = 0.0041 mol L^{-1}, HA supersaturation = 27.1, OCP supersaturation = 14.7, ΔG_{HA} = – 8266 J mol^{-1}, and ΔG_{OCP} = – 6824 J mol^{-1} were obtained. This homogenization of pH and other parameters occurs simultaneously with the complete coating of the metallic surface, as observed in Figure 5b. Figure 5a images the surface at the onset of immersion, with a clear metallic surface and the local pH-SME sensor.

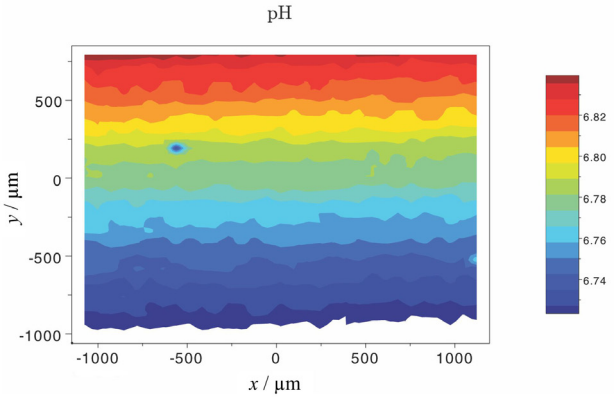

Figure 4. Experimental local pH map after 44 h.

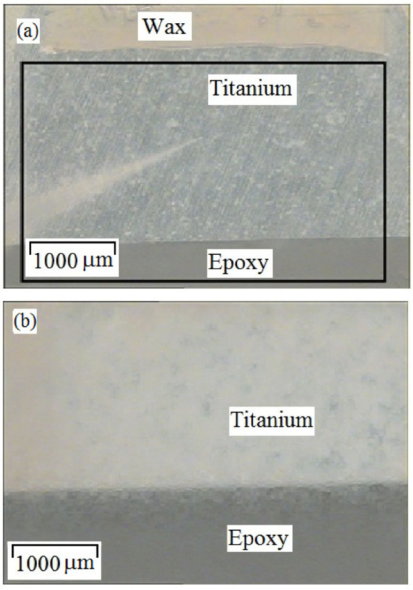

Figure 5. Optical images of titanium, taken *in situ* at SIET equipment, surrounded by a passive area of wax and epoxy holder. (a) Surface of titanium and wax during the first instants. The pH-microelectrode can be seen at ca. 45° from the wax-Ti interface towards the center. The black rectangle shows the area of the pH scan. (b) Surface after 44 h exposure, with a final thick deposit on titanium.

The calcium content in solution is frequently monitored in order to detect, and even quantify, the ability of apatite to deposit on surfaces, known as a bioactivity test. In this way, the decrease of calcium content in solution is considered to be a heterogeneous

precipitation, mainly on the metallic substrate.[18] However, for calcium phosphates immersed in SBF for up to 7 days, an interesting result of calcium availability was detected: the calcium content in solution increased for up to 6 h, and subsequently dropped.[19] One possible explanation for the cyclic variations in the local pH on surface of the titanium may be described as follows. Initially, the deposition of the first layers of apatite on the metallic surface occurs along with some evolution of CO_2 owing to carbonate/bicarbonate/carbon dioxide reactions.

The reactions of carbon dioxide in aqueous medium can be expressed in equations 14-16:

$$CO_2(g) \rightleftharpoons CO_2 \text{ (aqueous)}, \quad (14)$$

$$CO_2 \text{ (aqueous)} + H_2O \rightleftharpoons H_2CO_3, \quad (15)$$

$$H_2CO_3 \rightleftharpoons H^+ + HCO_3^-. \quad (16)$$

Moreover, the equilibrium reaction between gaseous carbon dioxide and aqueous carbon dioxide is represented by:[20]

$$K_{eq} = \frac{a_{CO_2}}{\phi_{CO_2} p_{CO_2}}, \quad (17)$$

where ϕ_{CO_2} refers to the fugacity coefficient for carbon dioxide in the gaseous phase, a_{CO_2} is the activity of carbon dioxide in the liquid phase and p_{CO_2} is the partial pressure of carbon dioxide. The fugacity coefficient for carbon dioxide is evaluated using the expression:[20]

$$\log\phi_{CO_2} = P(0.0031 - 1.4/T), \quad (18)$$

where T is the absolute temperature (Kelvin) and the pressure P is measured in bar. Clearly, the gaseous carbon dioxide partial pressure must be specified in order to solve equation 17. In an additional simulation, the effect of carbon dioxide partial pressure in the range $0 \leq p_{CO_2} \leq 0.10$ bar was studied, as shown in Figure 6, which is the range of biomedical interest. It is worth noting that this calculation was done considering all equilibrium reactions 1-11 plus 14-18.

Therefore, the observed local pH increases slightly and simultaneously the initial precipitation on metal occurs. The local pH evolution up to 5 h can be speculated as a consequence of carbon dioxide release. After a period of approximately 5 h, and on the top of the initial calcium phosphate layer, deposition takes place at a more intense rate due to its similarity to the new substrate of apatite. The more intense fixation of phosphate as hydroxyapatite reduces the local hydroxide ion concentration and consequently the pH drops, as observed in Figure 2.

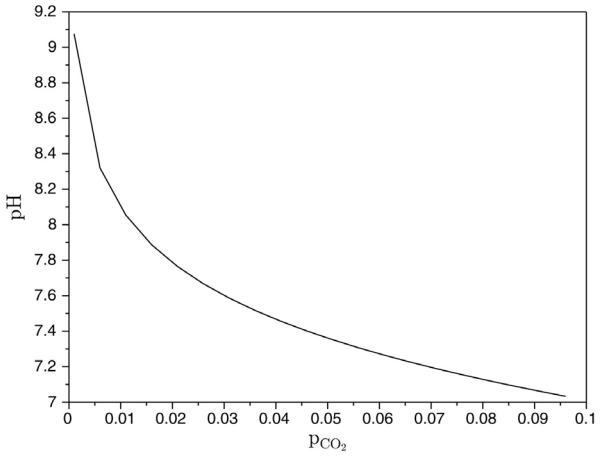

Figure 6. pH evolution as a function of CO_2 content.

The numerical simulations allow access to a large number of necessary quantities (ionic concentrations, supersaturations, etc.); therefore, any algebraic manipulation (as used by Carey and Vogel) was not used.[21] Besides, the visualization of concentration maps is always available even for a more complex system (with more uncommon species).

Conclusions

A detailed map of local pH during biomimetic deposition on biomedical grade titanium was obtained by using the ion-selective microelectrode technique. The averaged local pH presents an increase-decrease cycle, with a turning point at 5 h. From the local pH measurements, and taking into account the chemical equilibrium in the liquid phase, it was possible to obtain maps corresponding to all species in solution. The numerical simulation of supersaturation and free Gibbs energy variation of hydroxyapatite and octacalcium revealed that the monitoring of a single parameter (i.e., pH or free calcium concentration) is not capable of predicting the tendency for calcium phosphate precipitation. On the other hand, local measurements, along with computational simulations, provide an adequate visualization of conditions of the biomimetic precipitation.

Acknowledgements

The authors acknowledge the financial support of Brazilian agencies Conselho Nacional de Desenvolvimento Científico e Tecnológico (CNPq), Coordenação de Aperfeiçoamento de Pessoal de Nível Superior (CAPES) and Fundação Carlos Chagas Filho de Apoio à Pesquisa do Estado do Rio de Janeiro (FAPERJ). G. M. Platt, I. N. Bastos and M. C. Andrade acknowledge Universidade do Estado do Rio de Janeiro (UERJ) for their ProCiencia Grants. S. Lamaka and M. Tariba acknowledge

financial support from 7th Framework Programme for Research and Technological Development (FP7) Marie Curie International Research Staff Exchange Scheme (IRSES), project Enhancing Scanning Ion-Selective Electrode Technique (SISET). M. Tariba gratefully thanks Fundação para a Ciência e Tecnologia (FCT/Portugal) for her PhD grant SFRH/BD/72602/2010.

References

1. Cigala, R. M.; Crea, F.; Stefano, C.; Lando, G.; Manfredi, G.; Sammartano, S.; *J. Mol. Liq.* **2012**, *165*, 143.
2. Bastos, I. N.; Platt, G. M.; Andrade, M. C.; Soares, G. D.; *J. Mol. Liq.* **2008**, *139*, 121.
3. Glinkina, I. V.; Durov, V. A.; Mel'nitchenko, G. A.; *J. Mol. Liq.* **2004**, *110*, 63.
4. Resende, C. X.; Dille, J.; Platt, G. M.; Bastos, I. N.; Soares, G. A.; *Mater. Chem. Phys.* **2008**, *109*, 429.
5. Protocol ISO/CD 23317 2005: *Implants for Surgery - In vitro Measurement of Apatite forming Ability of Implant Materials*.
6. Resende, C. X.; Pagano, R. L.; Calado, V. M. A.; Bastos, I. N.; Biscaia, E. C.; Soares, G. A.; *Int. Rev. Chem. Eng. Rapid Commun.* **2010**, *2*, 748.
7. Marenzana, M.; Shipley, A. M.; Squitiero, P.; Kunkel, J. G.; Rubinacci, A.; *Bone* **2005**, *37*, 545.
8. Lamaka, S. V.; Taryba, M.; Montemor, M. F.; Isaacs, H. S.; Ferreira, M. G. S. *Electrochem. Commun.* **2011**, *13*, 20.
9. Alvarez-Pampliega, A.; Lamaka, S. V.; Taryba, M. G.; Madani, M.; De Strycker, J.; Tourwé, E.; Ferreira, M. G. S.; Terryn, H.; *Electrochim. Acta* **2012**, *61*, 107.
10. Berger, C. E. M.; Horrocks, B. R.; Datta, H. K.; *Electrochim. Acta* **1999**, *44*, 2677.
11. International Union of Pure and Applied Chemistry; *Pure Appl. Chem.* **1997**, *69*, 1325.
12. Larson, T. E.; Sollo Jr., F. W.; McGurk, F. F.; Water Resources Center Report 68: *Complexes Affecting the Solubility of Calcium Carbonate in Water*; University of Illinois, Water Resources Center: Illinois, USA, 1973.
13. Chugtai, A.; Marshall, R.; Nancollas, G. H.; *J. Phys. Chem.* **1968**, *72*, 208.
14. Cotton, F. A.; Wilkinson, G.; *Advanced Inorganic Chemistry*, 5th ed.; Wiley: New York, USA, 1988.
15. Lu, X.; Leng, Y.; *Biomaterials* **2005**, *26*, 1097.
16. Dorozhkin, S. V.; *Acta Biomater.* **2010**, *6*, 4457.
17. Tung, M. S.; Eidelman, N.; Sieck, B.; Brown, W. E.; *J. Res. Natl. Bur. Stand.* **1988**, *93*, 613.
18. Vanzillotta, P. S.; Sader, M. S.; Bastos, I. N.; Soares, G. A.; *Dent. Mater.* **2006**, *22*, 275.
19. Monteiro, M. M.; Rocha, N. C. C.; Rossi, A. M.; Soares, G. A.; *J. Biomed. Mater. Res. Part A* **2003**, *65*, 299.
20. Platt, G. M.; Bastos, I. N.; Andrade, M. C.; Soares, G. D. A.; *Adv. Mater. Chem. Phys.* **2012**, *2*, 239.
21. Carey, C. M.; Vogel, G. L.; *J. Res. Natl. Inst. Stand. Technol.* **2000**, *105*, 267.

Submitted: January 7, 2013
Published online: June 5, 2013